ACS Catalysis

Research Article

pubs.acs.org/acscatalysis

Mechanism of *n*-Butane Hydrogenolysis Promoted by Ta-Hydrides Supported on Silica

Farhan Ahmad Pasha, Luigi Cavallo,* and Jean Marie Basset*

KAUST Catalysis Center (KCC), Physical Sciences and Engineering Division, King Abdullah University of Science and Technology, Thuwal 23955-6900, Saudi Arabia

Supporting Information

ABSTRACT: The mechanism of hydrogenolysis of alkanes, promoted by Ta-hydrides supported on silica via 2 ≡Si−O− bonds, has been studied with a density functional theory (DFT) approach. Our study suggests that the initial monohydride $(\equiv Si-O-)_2Ta^{(III)}H$ is rapidly trapped by molecular hydrogen to form the more stable tris-hydride $(\equiv Si-O-)_2Ta^{(V)}H_3$. Loading of *n*-butane to the Ta-center occurs through C−H activation concerted with elimination of molecular hydrogen (*σ*-bond metathesis). Once the Ta-alkyl species is formed, the C−C activation step corresponds to a *β*-alkyl transfer to the metal with elimination of an olefin. According to these calculations, an *α*-alkyl transfer to the metal to form a Ta-carbene species is of higher energy. The olefins formed during the C−C activation step can be rapidly hydrogenated by both mono- and tris-Ta-hydride species, making the overall process of alkane cracking thermodynamically favored.

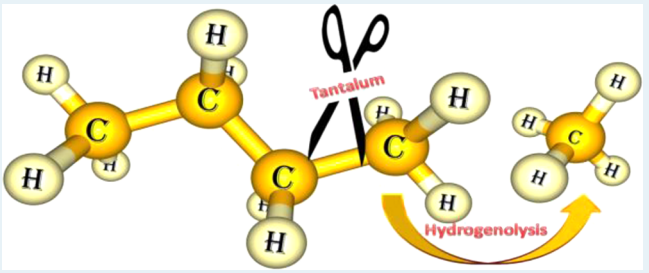

KEYWORDS: *surface organometallic chemistry, tantalum, alkanes, hydrogenolysis, density functional theory, silica*

INTRODUCTION

Low-temperature hydrogenolysis of saturated hydrocarbons is a field of considerable interest in the petrochemical sector to generate valuable chemicals and hydrocarbons from higher alkanes,[1] with a potential expanding to the depolymerization of polyolefin via the microscopic reverse of Ziegler−Natta polymerization.[2] There are several known catalysts, mainly based on late transition metals, such as Ni, Pt, Rh, Re, etc., but they often require rather high temperatures to work effectively.[3] This drawback has motivated the search for alternative catalysts that might operate under milder conditions. In this context, hydrides of early transition metals supported on various oxides have shown unprecedented and striking activity,[2,4] including dinitrogen activation and hydrogenolysis of alkanes. More specifically, Ta-hydrides have shown activity for N_2 splitting,[5] alkane metathesis,[6] as well as for hydrogenolysis of light alkanes[7] and cyclic alkanes,[8] aromatic C−H activation[9] and we recently showed that the hydrogenolysis of a mixture of alkanes over Ta-hydrides supported on MCM-41 leads to the formation of propane, ethane, and methane.[10] Remarkably, the developed catalysts efficiently catalyze the hydrogenolysis of alkanes at low temperature (T < 150 °C) and low atmospheric pressure (P < 1 atm). The reaction proceeded with good catalytic activity, TONs, and stability. Notably, the reaction was conducted in a dynamic reactor, and the catalyst was found to have an impressive ability to be regenerated and reused several times, which makes the overall catalytic process sustainable. The potential shown by these catalysts induced us to start a detailed characterization and mechanistic understanding of these catalysts at work.[5,7,10,11]

Focusing on the structure of the active species, the formation of silica-supported bipodal tantalum monohydride, of general formula $[(\equiv SiO)_2TaH]$, with the metal present as a highly unsaturated $Ta^{(III)}$ center, is known.[12] Furthermore, it has been recently found that, in the presence of molecular hydrogen, the monohydride $[(\equiv SiO)_2TaH]$ could be in equilibrium with the trihydride of general formula $[(\equiv SiO)_2TaH_3]$, where the metal is present as a saturated $Ta^{(V)}$ center.[5] However, despite this knowledge of the nature of the active species, the possible mechanism through which the grafted Ta-hydride(s) performs alkane hydrogenolysis is still unclear. In continuation of our study,[10] here, we report viable mechanisms of C−C bond hydrogenolysis in alkanes, based on DFT calculations.

To model the Ta-active species, we used clusters similar to those of Figure 1. As a model for linear alkanes, we used *n*-butane. Experimentally, it was shown that with Ta/MCM-41 it is possible to perform the hydrogenolysis of *n*-butane, with a product distribution consisting of methane, ethane, and propane, with ratios of ca. 40/35/25 at high conversion.[10]

As final note, we recall here that a striking difference exists between $[(\equiv SiO)_3ZrH]$ and $[(\equiv SiO)_2TaH_3]$. The Ta hydride is able to cleave the C−C bond of ethane to give methane, whereas the Zr hydride does not give methane.[13] This was explained considering that Ta hydrides can promote *α*-alkyl, transfer to the metal, with formation of a tantalum (alkyl) (carbene) species, a reactivity, which is not possible with a

Received: February 10, 2014
Revised: April 21, 2014
Published: April 23, 2014

   dx.doi.org/10.1021/cs5001703 | ACS Catal. 2014, 4, 1868−1874

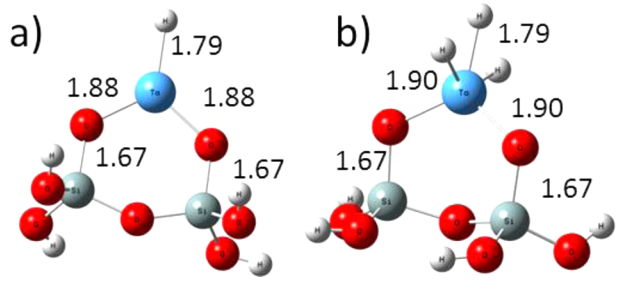

Figure 1. Optimized geometry of the clusters used to model (a) $[(\equiv SiO)_2TaH]$ and (b) $[(\equiv SiO)_2TaH_3]$. Distances given in Ångstroms.

tripodal $[(\equiv SiO)_3ZrH]$ or even with a bipodal $[(\equiv SiO)_2ZrH_2]$.[13]

COMPUTATIONAL DETAILS

Cluster Calculation. All the calculations have been performed using the M06 density functional,[14] as implemented in the Gaussian09 package.[15] The triple-ζ basis set TZVP[16] was used for main group elements, while for Ta we used the small-core, quasi-relativistic Stuttgart/Dresden effective core potential with the associated valence SDD basis set.[17] Singlet and triplet spin multiplicity were compared for the initial mono- and tris-hydride Ta-species. Since, in both structures, the singlet state was clearly more stable, the entire study was performed assuming a singlet spin state. All stationary points were characterized through frequency calculations. The reported energies correspond to Gibbs energies calculated under the ideal gas approximation, at 298.15 K and 1 atm, unless specified otherwise. Since we discuss several, heavily interconnected, reaction pathways, we decided to assume the tris-hydride Ta-species of Figure 1 plus *n*-butane and H_2 as the reference state at 0 kcal/mol. All of the other species are thus presented relative to this reference state, by adding/subtracting the energy of the hydrogen, methane, ethane, ethene, propene, and butane molecules needed to connect chemically the species under discussion with the assumed reference state.

Periodic Calculations. The silica-supported bipodal Ta-species was simulated using a periodic approach. The coordinates for the optimized silica were obtained from the literature[18] and a 2 × 2 super cell was constructed with the Ta atom anchored between two silanols. Five SiO_2 layers were considered perpendicular to the surface. The box size of 13.59 Å × 13.62 Å × 35 Å was kept fixed during the entire simulation and the bottom three layers were frozen during the simulation. The periodic DFT calculations were performed using a plane wave approach, as implemented in the VASP[19] 5.3 code. The GGA PBE exchange−correlation functional of Perdew−Burke−Ernzerhof was used.[20] The projector augmented plane wave[21] (PAW) approach was used to describe the interactions between the core and the valence electron. The energy cutoff for the plane-wave basis set expansion was set to 400 eV. The Brillouin zone was sampled with a 2 × 2 × 1 Monkhorst−Pack *k*-point grid. Besides minima, we analyzed the transition states using a nudged elastic band (NEB) approach, as implemented in VASP. There were eight intermediate frames defined between two stationary points. The other parameters were kept at the default value, as defined in VASP. The ion coordinates were optimized up to residual forces within 0.01 eV/A. All of the energies used here are total electronic energies without any entropic correction.

Results. Considering that the small SiO cluster used in this work could allow high and unphysical flexibility around the Ta center, first we compare *n*-butane addition and the following C−H cracking step using a periodic model, and then made comparison with the cluster model.

Periodic DFT Calculations. The energy describing the loading of *n*-butane onto the tris-hydride species **2**, leading to the Ta-butyl bis-hydride species **3** and **4**, as obtained with the cluster model and the periodic model, respectively, are compared in Figure 2. As a remark, we compare electronic energies rather than Gibbs energies in Figure 2,

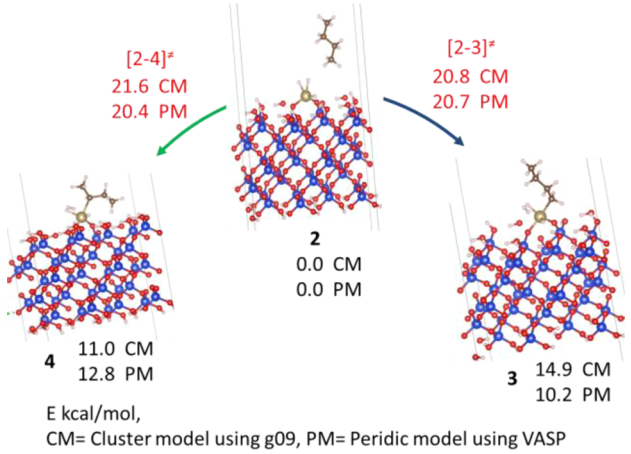

Figure 2. Comparison of the energetics of the C−H bond activation of *n*-butyl Ta-species **3**, using a periodic model (PM values in the figure) and a cluster model (CM in the figure). The electronic energy (in kcal/mol) of the intermediates (in black) and of the transition state connecting them (in red) are reported in parentheses.

because no vibrational analysis was performed with the periodic model. The data reported in Figure 2 clearly indicate a substantial agreement between the cluster model and the periodic model, both in terms of the relative stability of the various intermediates, as well as in the energy barriers connecting them, validating calculations performed with the cluster model. On the other hand, the periodic model has an obviously much greater computational cost, making unpractical to use it to model the large number of reactions considered in this work.

In conclusion, in agreement with similar tests on N_2 dissociation on an isolated surface Ta-atom,[22] our tests indicate that very similar results, and basically the same chemical scenario, is provided by the cluster model and the periodic model.

Catalyst Initiation and Substrate Activation. We start with a comparison of the relative stability of $[(\equiv SiO)_2Ta^{(III)}H]$ (**1**, which is a d^2 species presenting a highly unsaturated $Ta^{(III)}$ center), and the $Ta^{(V)}$ d^0 specie **2** shown in Figure 3. As a remark, the M06 functional that we used here predicts that the preferred electronic state for the monohydride species is a singlet, with the triplet 4.2 kcal/mol higher in energy. This is different from what has been reported in the literature, where the triplet is found to be more stable than the singlet.[5] Indeed, test calculations performed with the BP86, B3LYP, B3PW91, and M06L functionals, consistently predict the triplet state to be more stable than the singlet by 1−5 kcal/mol. However, an in-depth investigation of this point is beyond the scope of the present work, and we used the singlet state of the monohydride in the following discussion.

Consistent with previous calculations,[5,10] the tris-hydride $[(\equiv SiO)_2Ta^{(V)}(H)_3]$ **2** is the most stable species, laying 26.7 kcal/mol below **1**, and 9.1 and 8.9 kcal/mol below the Ta-butyl species (**3** and **4**, respectively), according to the computational protocol used in this work. The higher stability of **4**, relative to **3**, can be explained considering a more σ-donating character of the secondary alkyl in **4**. For this reason, in the following, we will consider **2** as the reference structure at 0.0 kcal/mol in energy. The tris-hydride **2** can be reached from **1** through the addition of H_2, which is a barrierless event on the potential energy surface, while it might have an entropically driven barrier on the Gibbs energy surface.[23] Differently, oxidative addition of butane to **1**, through the C−H activation transition states $[1-3]^{\ddagger}$ and $[1-4]^{\ddagger}$, located 46.9 and 46.4 kcal/mol above **2**, has a clear energy barrier of roughly 20 kcal/mol from **1** (see Figure 3). Next, we explored the possibility of *n*-butane C−H activation promoted by **2**.

Two possible mechanisms can be envisaged for loading *n*-butane to **2**: the first consists of a concerted σ bond metathesis (C−H activation/H_2 elimination) through transition state $[2-3]^{\ddagger}$ or $[2-4]^{\ddagger}$, as depicted in Figure 3; and the second is a two-step reaction, consisting of regeneration of the monohydride **1**, followed by oxidative

dx.doi.org/10.1021/cs5001703 | ACS Catal. 2014, 4, 1868−1874

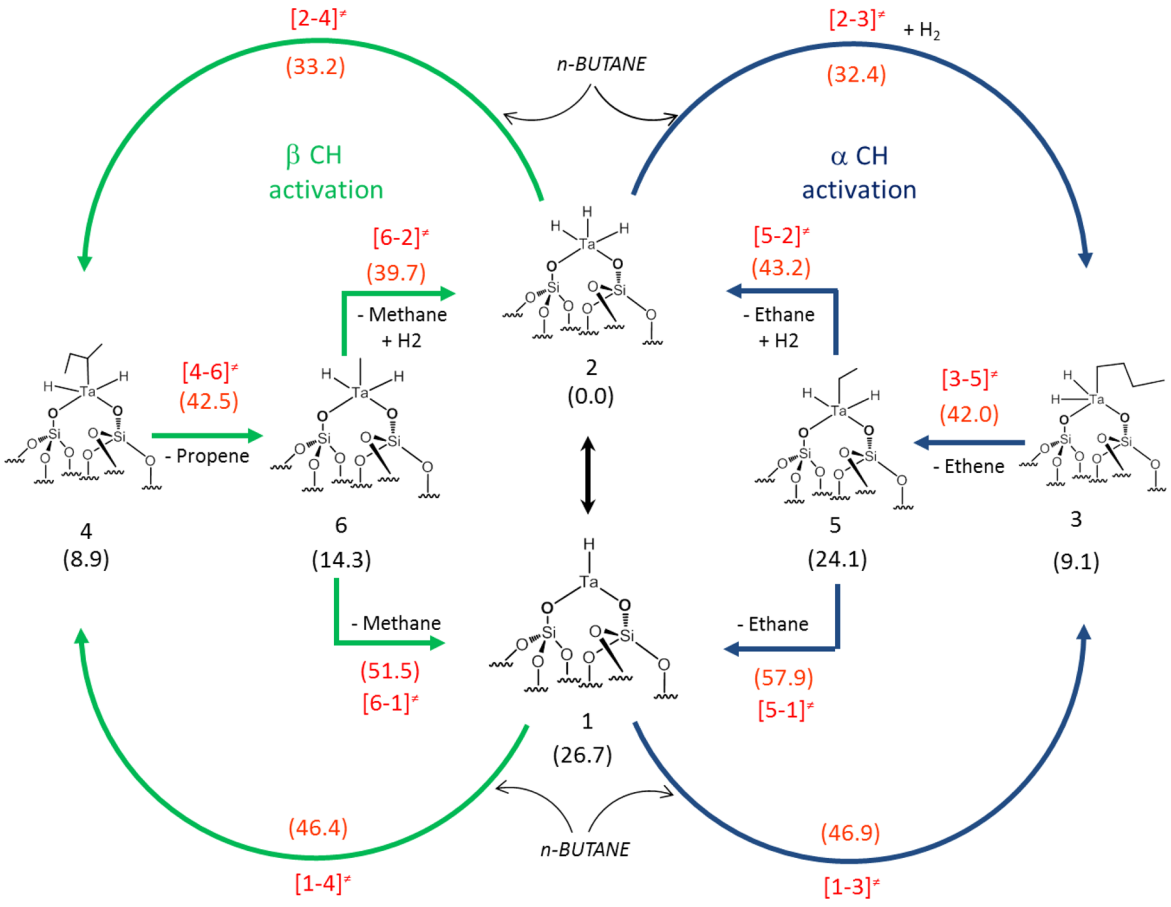

Figure 3. Energy profile for the interconversion of the mono- and tris-hydride Ta-species, and for hydrogenolysis of *n*-butane. The blue cycle corresponds to α-CH activation and the green cycle corresponds to β-CH activation. Gibbs energies (in kcal/mol) of the intermediates (in black) and of the transition state connecting them (in red) are reported in parentheses.

addition of butane through the previously discussed transition state ($[1-3]^{\ddagger}$ or $[1-4]^{\ddagger}$). According to calculations, the concerted C−H activation/H_2 elimination mechanism is clearly favored, since transition states $[2-3]^{\ddagger}$ or $[2-4]^{\ddagger}$ are ∼32 kcal/mol above **2**, whereas transition states $[1-3]^{\ddagger}$ and $[1-4]^{\ddagger}$, are more than 14 kcal/mol higher in energy. Activation of a terminal C−H bond, leading to the linear Ta-alkyl species **3**, is kinetically slightly favored over formation of the branched Ta-alkyl species **4**, which indicates a scarcely selective C−H activation, favoring formation of the linear Ta-butyl species **3**.

C−C Activation from the Linear Ta-Butyl Species 3. Activation of the Cβ−Cγ bond of **3** (β-alkyl transfer), to eliminate ethene and give the bis-hydride Ta-ethyl intermediate **5**, 15.0 kcal/mol above **3** (see Figure 3), occurs through transition state **3**−**5** with a barrier of 32.9 kcal/mol from **3**. This is an endoergonic step, because of the formation of the high-energy ethene molecule from the *n*-butyl Ta ligand, and it basically corresponds to a depolymerization step. However, the energy penalty associated with this step will be largely recovered by rapid insertion of the formed ethene into one of the largely present Ta-hydride bonds (see later discussion). Indeed, the driving force for the reaction is the Gibbs energy balance of the overall hydrogenation of *n*-butane to two ethane molecules, which is favorable by 15.2 kcal/mol at the level of theory considered in this work.

Transition state $[3-5]^{\ddagger}$ presents an almost-octahedral geometry at the Ta-center (see Figure 4), with the two hydride ligands in trans position. Transition state $[3-5]^{\ddagger}$ is rather similar to the transition state for ethene insertion into a Ta-alkyl bond, with related mono- and tripodal Ta-silica species.[24] As the transition state is reached, ethene is expelled from the Ta-center, and the preferred trigonal bipyramid geometry is restored. Consistent with the mechanism proposed for alkane hydrogenolysis on silica-supported Zr-species,[25] this step is best

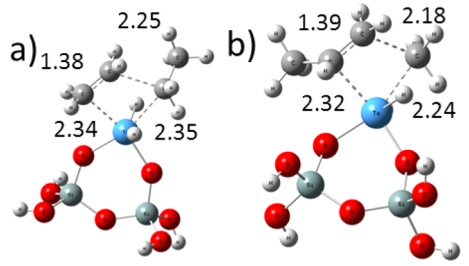

Figure 4. Geometry of transition states (a) $[3-5]^{\ddagger}$ and (b) $[4-6]^{\ddagger}$; all distances given in Ångstroms.

described as a β-alkyl transfer to the metal. On this point, we remark that, normally, two trans-oriented hydride ligands in this type of complex is not the preferred geometry.[11a] Indeed, we found that, at the level of the intermediates **3** and **4**, the trans-hydride geometry is 1 kcal/mol less stable than a cis-oriented geometry. However, at the level of transition state $[3-5]^{\ddagger}$, the geometry with a trans-orientation of the hydrides is preferred by at least 2 kcal/mol. Incidentally, with trans-hydrides, the alkyl groups would be oriented away from the SiO_2 surface, eventually minimizing steric interaction with the surface. Similar considerations can be applied to transition state $[4-6]^{\ddagger}$ of Figure 3.

Elimination of ethane from intermediate **5** can proceed along two possible reaction pathways. The first corresponds to simple reductive elimination of ethane through transition state $[5-1]^{\ddagger}$, laying 33.8 kcal/mol above **5**. The second corresponds to ethane elimination assisted by an external H_2 molecule, and it is can considered as an easy step, since transition state $[5-2]^{\ddagger}$ lies only 19.1 kcal/mol above **5** (see

dx.doi.org/10.1021/cs5001703 | ACS Catal. 2014, 4, 1868−1874

Figure 3). Comparison between the two pathways indicates that the latter is strongly preferred, which is reasonable, considering that it prevents the formation of the highly unsaturated monohydride species **1**.

Another possible pathway for alkanes hydrogenolysis promoted by Ta-catalysts was proposed by us in 2000,[13a] and was hypothesized to proceed through a σ-bond metathesis. We tried to locate this transition state similar to Figure 5a; however, in all of our attempts, the system

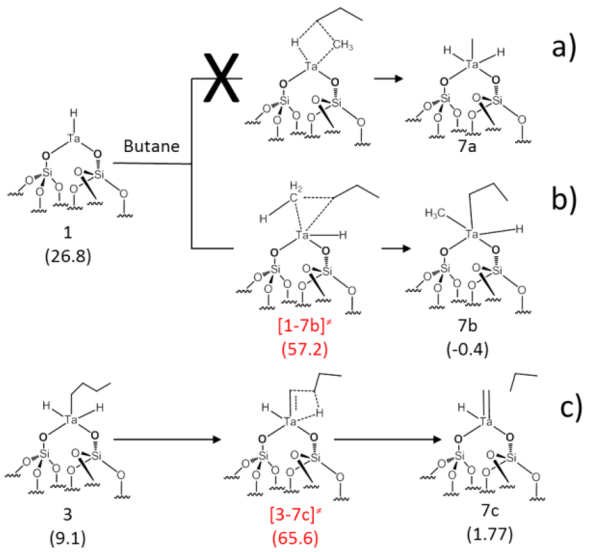

Figure 5. Alternative mechanisms for C−C cleavage. Gibbs energies (in kcal/mol) of the intermediates (in black) and of the transition state connecting them (in red) are reported in parentheses.

collapsed into a monohydride and bis-alkyl $Ta^{(V)}$ species 7b with a high barrier of 57.2 kcal/mol, as presented in Figure 5b. The high barrier (57.2 kcal/mol), in comparison to the pathway low-energy barrier (42.0 kcal/mol), presented in Figure 3, ruled out this possibility. Furthermore, as an alternative to the β-alkyl transfer mechanism of Figure 3, we explored the possibility of direct propane formation through transfer of a Ta hydride of **3** to the β carbon of the Ta-butyl moiety, along with the release of propane and the formation of the Ta-carbene species **7c** shown in Figure 5c.

This step, occurring through a concerted four-centers transition state, has the high barrier of 65.5 kcal/mol, compared to the 42.0 kcal/mol calculated for the β alkyl transfer to the metal, ruling out this possibility.

In conclusion, the preferred C−C activation mechanism cracks *n*-butane to ethane + ethene, regenerating the tris-hydride species **2**, through a β-alkyl transfer mechanism. This cracking step is calculated to be endoergonic by 12.1 kcal/mol. However, rapid hydrogenation of the formed ethene molecule to ethane by any of the plethora of Ta−H bonds in the system (see later discussion) makes the overall process exoergonic. As for the height of the energy barrier for the productive pathway, 42.0 kcal/mol, it certainly is a high energy barrier even at 150 °C, which indicates that our calculated value somehow overestimates the real energy barrier for this process.

Other Reactivity Started from the Linear Ta-Butyl Species 3. The other possible reactivity we considered for **3** as starting species are shown in Figure 6. They correspond to the activation of the Cα−H and Cβ−H bonds of the Ta-butyl species **3**, to give the Ta-carbene species **8**, and the tantalacycloalkane species **9**, **10**, and **11**, all cases occurring with the elimination of H_2. Keeping in mind that transition state $[3-5]^{\ddagger}$, corresponding to the C−C activation step, resides at 42.0 kcal/mol (see Figure 3), Cα-H activation leading to the Ta-carbene species **8**, through transition state $[3-8]^{\ddagger}$ at 44.2 kcal/mol, is slightly disfavored, relative to the C−C activation step $[3-5]^{\ddagger}$, while Cβ−H or Cδ−H activation to the Ta-cycloalkane species **9** and **11**, through transition state $[3-9]^{\ddagger}$ and $[3-11]^{\ddagger}$ at 30.9 and 36.8 kcal/

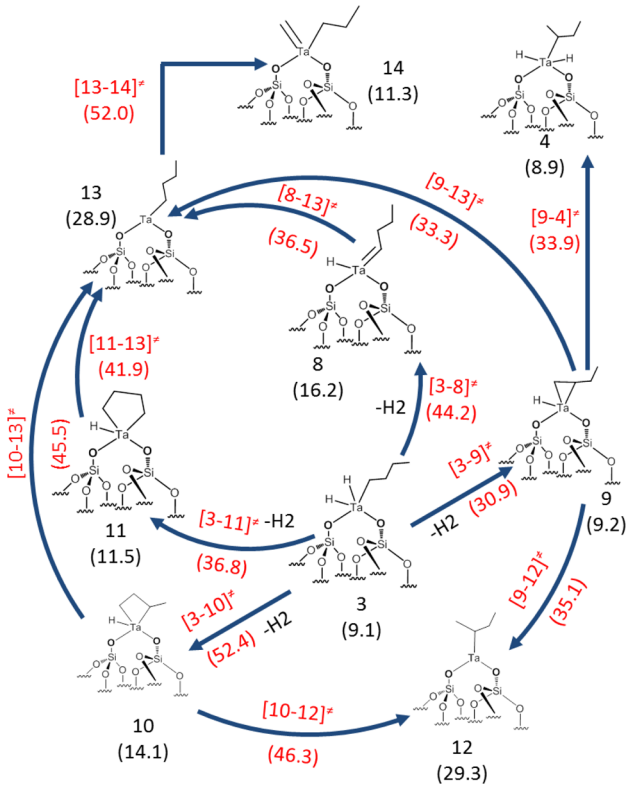

Figure 6. Possible reactivity starting with the activation of a C−H bond of the *n*-butyl Ta-species **3**. Gibbs energies (in kcal/mol) of the intermediates (in black) and of the transition state connecting them (in red) are reported in parentheses.

mol, is clearly preferred. Differently, Cγ−H activation to the Ta-cyclobutane species **10**, through transition state $[3-10]^{\ddagger}$ at 52.4 kcal/mol, can be excluded. The formed intermediates **8**, **9**, and **11** can either react backward with H_2 to regenerate **3**, or proceed further to form the high-energy Ta(III) monoalkyl species **12** and **13**, re-entering the C−C breaking cycle. Noteworthy, the pathways shown in Figure 6 also indicate possible isomerization routes converting the *n*-butyl Ta species **3** into the isobutyl Ta species **12**, which is an additional step that can impact the final distribution of the products. Alkyl Cα-transfer from the Ta-butyl species **13** to give the Ta(methylidene)(*n*-propyl) species **20** occurs through the high-energy transition state $[13-14]^{\ddagger}$, laying at 52.0 kcal/mol. Considering that H_2 addition to **13** is practically barrier less, and that **13** can be easily reversed to **8**, **9**, or **11** through transition states clearly lower in energy than $[13-1]^{\ddagger}$, C−C breaking through α-alkyl transfer is not competitive with the β-alkyl transfer discussed in the previous section.

While the above results indicate that the most favorable C−C breaking step occurs through β-alkyl transfer to the metal, they also indicated that several transformations of the Ta-butyl species **3** are clearly favored relative to the β-alkyl transfer. For example, β-H transfer with concerted H_2 elimination to give the Ta-metallacycle **9** proceeds through the lower-energy transition state $[3-9]^{\ddagger}$. However, the foreseeable evolution of **9** is to the $Ta^{(III)}$-butyl species **12** or **13**, which means reintroducing **9** into the main catalytic cycle. There is another possibility by introducing external hydrogen, so that **9** may transform into **4** via transition state $[9-4]^{\ddagger}$, but this barrier is 33.9 kcal/mol. This indicates that the Ta species could undergo a remarkable number of nonproductive reactions, with the proposed productive β-alkyl transfer a rare event in comparison. An example of this type of reactivity is in the nonproductive degenerate metathesis of olefins promoted by Ru-catalysts.[26] Overall, these results indicate that, after the substrate is loaded onto the catalyst, it can equilibrate in many different species, as shown in Figure 6, with the most stable intermediate corresponding to the bis-hydride $Ta^{(V)}$-alkyl species **3**

dx.doi.org/10.1021/cs5001703 | ACS Catal. 2014, 4, 1868−1874

(or, by barrierless H_2 addition to **12**, to the analogous Ta-species **4**). Evolution of these intermediates is through the C−C breaking β-alkyl transfer of Figure 3.

C−C Activation from the Branched Ta-Butyl Species 4. Activation of the Cβ−Cγ bond of **4** eliminates propene and give the bis-hydride Ta-methyl intermediate **6**, 5.4 kcal/mol above **4** (see Figure 3). This is again an endoergonic step, because of the formation of a high-energy propene molecule from the *i*-butyl ligand, which will be compensated by hydrogenation of the formed propene. Formation of **6** occurs through transition state $[4-6]^{\ddagger}$ with a barrier of 33.6 kcal/mol from **4**, which is only 0.7 kcal/mol higher than the barrier for the Cβ−Cγ activation step from **3** (see Figure 3). Also, in this case, the following methane liberation step assisted by a H_2 molecule to regenerate the tris-hydride Ta-species **2**, through transition state $[6-2]^{\ddagger}$, is clearly favored than simple reductive elimination of methane, to give the monohydride Ta-species **1** through transition state $[6-1]^{\ddagger}$. Consistently with C−C activation from the linear Ta-butyl species **3**, transition state $[4-6]^{\ddagger}$ presents an almost-octahedral geometry at the Ta-center, with the two hydride ligands in trans (see Figure 4b), and can be classified as classic β-methyl transfer to the metal. It can be also considered as the transition state for secondary insertion of propene into a Ta-methyl bond, and the methyl of propene is placed in an open part of space, with minimal steric repulsion with other groups at the catalytic site, as typical in propene polymerization.[27] Also in this case, the olefin is expelled from the Ta-center as it is formed.

In conclusion, the preferred C−C activation mechanism from the Ta-isobutyl moiety cracks *n*-butane to propene + methane, regenerating the tris-hydride species **2**. Similarly to the cracking of *n*-butane to ethene and ethane, the C−C breaking step with formation of methane and propene is endoergonic, by 6.0 kcal/mol in this case. Hydrogenation of the formed propene to propane by the mono- or tris-hydride species **1** and **2** makes the overall process exoergonic.

Finally, comparison between β-alkyl transfer from the linear Ta-alkyl species **3**, through transition state $[3-5]^{\ddagger}$ at 42.0 kcal/mol, and the branched Ta-alkyl species **4**, through transition state $[4-6]^{\ddagger}$ at 42.5 kcal/mol, again indicates low selectivity in the hydrogenolysis of *n*-butane, which is consistent with the experimental results.

Other Reactivity Started from the Branched Ta-Butyl Species 4. The other possible reactivity, by considering **4** as the starting species, is shown in Figure 7. It corresponds to activation of the Cα−H and of the internal Cβ−H bonds of the Ta-butyl species **4**, to give the Ta-carbene species **15**, and the tantalacyclopropane species **16**, in both cases with elimination of H_2. We did not consider activation of the methyl Cβ−H bond, since it would lead to the Ta-cyclopropane species **9**, a case already considered in Figure 6, and we did not consider activation of the Cγ−H bond of **4**, giving a tantalacyclobutane intermediate, since we assume this to be a high-energy step, based on the results reported in Figure 6.

Focusing on the considered C−H activation steps, and keeping in mind that transition state $[4-6]^{\ddagger}$, corresponding to the C−C activation step, is observed at 42.5 kcal/mol (see Figure 3), Cα−H activation leading to the Ta-carbene species **15**, through transition state $[4-15]^{\ddagger}$ is competitive with the C−C activation step of Figure 3, while the Cβ−H activation to the Ta-cyclopropane species **16**, through transition state $[4-16]^{\ddagger}$ at 33.2 kcal/mol, is clearly preferred. Thus, also in case of the branched Ta-butyl species, the productive C−C activation step of Figure 3 is clearly slower than other nonproductive isomerization pathways. Using the $Ta^{(III)}$ species **12** as a representative system, we also investigated if C−C activation could occur with a mechanism different from those of Figure 3, specifically through an α-alkyl transfer to the metal, leading to the formation of Ta-carbene species such as **17** and **18** in Figure 7. These transformations could possibly result in low energy barrier, since they convert highly unsaturated $Ta^{(III)}$ species into saturated $Ta^{(V)}$ species.

However, the data reported in Figure 7 indicate that the formation of the Ta-carbene species **17** and **18** are rather high in energy transformations, since transition states $[12-17]^{\ddagger}$ and $[12-18]^{\ddagger}$ are ~50 kcal/mol in energy, although the specific barrier for the α-alkyl transfer step from **12** amounts to roughly 20 kcal/mol only. Even this barrier is too high, compared to the barrier for the backward

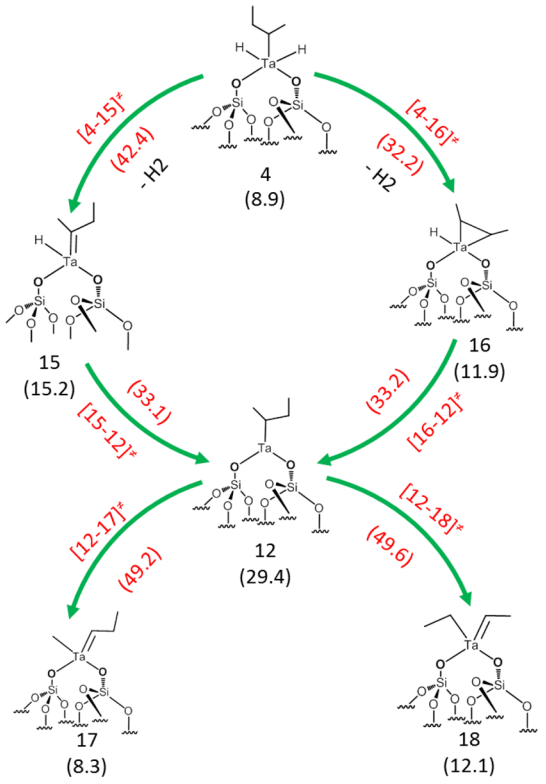

Figure 7. Possible reactivity starting with the activation of a C−H bond of the *i*-butyl Ta-species **4**. Gibbs energies (in kcal/mol) of the intermediates (in black) and of the transition state connecting them (in red) are reported in parentheses.

conversion of **12** to **15** and **16**, which amounts to only 5 kcal/mol. In conclusion, this suggests that the C−C activation step can only proceed through the β-alkyl transfer to the metal of Figure 3 (both blue and green cycles). Focusing on the closure of the catalytic cycle, an alternative to the mechanism proposed in Figure 3 could consist in intermediates **5** and **6** promoting C−H activation of another free *n*-butane molecule, with methane release through a σ-bond metathesis step, releasing ethane or methane and reforming an alkyl species. In this case, the trihydride Ta species **2** would not reform, and the Ta-butane will remain the key intermediate. We explored this possibility for the transformation from **6** to **3** (see Figure 8). However, these

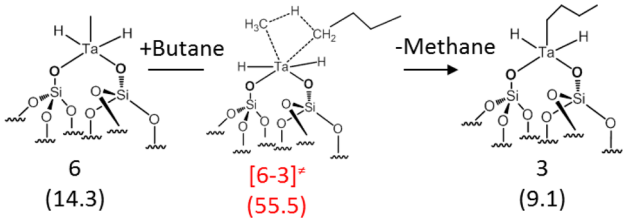

Figure 8. Alternative mechanism for catalytic cycle closure. Gibbs energies (in kcal/mol) of the intermediates (in black) and of the transition state connecting them (in red) are reported in parentheses.

possible results are unlikely, since the activation energy for this step, through transition state $[6-3]^{\ddagger}$, requires the high energy barrier of 55.5 kcal/mol, while methane release promoted by H_2, through transition state $[6-2]^{\ddagger}$, has a barrier of only 39.7 kcal/mol, respectively.

Reactivity of the Formed C=C Bonds. One peculiarity of the proposed mechanism for C−C activation from linear and branched Ta-butyl bonds is the formation of ethene and propene, as outlined in Figure 3. For this reason, we investigated the reactivity of ethene with

dx.doi.org/10.1021/cs5001703 | ACS Catal. 2014, 4, 1868−1874

the mono- and tris-hydrides Ta species **1** and **2** (see Figure 9), although we expected these processes to be of rather low energy. Reactivity with Ta-alkyl bonds is already comprised in Figure 3, if the reaction profiles are read backward.

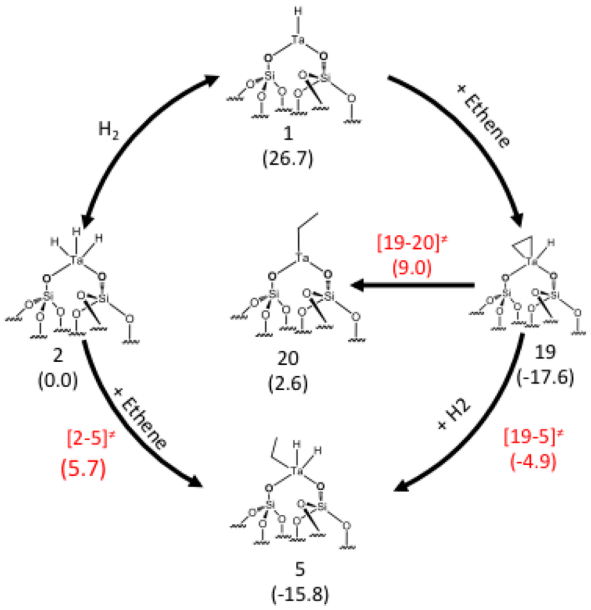

Figure 9. Reactivity of ethene with the mono- and tris-hydride Ta species **1** and **2**. Gibbs energies (in kcal/mol) of the intermediates (in black) and of the transition state connecting them (in red) are reported in parentheses.

In the case of the monohydride Ta-species **1**, ethene coordinates strongly to the Ta center, forming the tantalocyclopropane intermediate **19**, 44.3 kcal/mol below **1**. According to calculations, this is a barrierless event, which indicates that olefins can trap the monohydride Ta-species **1** as effectively as H_2 does. Intermediate **19** either can insert the coordinated ethene directly into the Ta−H bond through transition state $[19–20]^{‡}$ with a barrier of 26.7 kcal/mol, or can react with an external H_2 molecule, through transition state $[19–6]^{‡}$ and a barrier of only 12.8 kcal/mol.

Both pathways are clearly viable under the experimental conditions used, if the olefins formed during the C−C activation step (ethene and propene) are able to trap the monohydride species **1** before H_2. In the case of the tris-hydride Ta-species **2**, we could not find an ethene coordination intermediate, confirming again that the tris-hydride Ta-species is not willing to deform from a trigonal bipyramid geometry to an octahedral geometry to create the coordination position for the incoming olefin. Thus, there is direct insertion of ethene into one of the Ta−H bonds of **2**, with transition state $[3–5]^{‡}$ resembling those shown in Figure 4. The energy barrier for this transformation amounts to only 5.7 kcal/mol, and the low-energy intermediate **6** precipitates formed the systems. Overall, the ability of ethene to trap unsaturated $Ta^{(III)}$ species eventually present in the reactor, as well as the ability to insert into one of the plethora of the Ta−H bonds of any of the saturated $Ta^{(V)}$ species present in the reactor, could explain the absence of olefins in the products mixture.

An Overall View of Alkanes Hydrogenolysis on Ta-Hydride Species. The results achieved in this paper, combined with the computational results, relative to alkane hydrogenolysis discussed in a recent publication,[10] allows us to have a comprehensive view of the overall reactivity of alkanes in these systems. We briefly recall that, in the hydrogenolysis of alkanes, such as butane, on Ta-hydride complexes, the successive formation and disappearance of propane and ethane is observed, with methane as the only product at long reaction times.[13a] This overall behavior is consistent with the chemical scenario depicted by our calculations. The initial formation of ethane can be rationalized considering the Cβ-alkyl transfer discussed in Figure 3, which leads to the formation of ethene that is rapidly hydrogenated to ethane. The disappearance of ethane at longer reaction times can be rationalized by its hydrogenolysis through the energetically more expensive Cα-alkyl transfer mentioned in Figures 5 and 6 and discussed in detail in ref 10. Let us mention here that the reverse of this step is often considered as a critical step in Fischer−Tropsch synthesis, as well as in the nonoxidative coupling of methane to ethane and hydrogen.[2,11c]

Furthermore, the calculations reported in this manuscript allow us to have a more comprehensive picture of lower and higher alkanes hydrogenolysis promoted by Ta and by comparison Zr, silica-supported bipodal species. We recall the experimental evidence that ethane hydrogenolysis is not possible with Zr silica-supported bipodal species, while it is possible with the Ta analogues.[13] On the other hand, hydrogenolysis of butane was catalyzed by both Zr and Ta species. This induced us to hypothesize a different mechanism between Zr and Ta.[13,25]

Subsequent DFT calculations, together with those reported in this paper, suggest that the hydrogenolysis of higher alkanes, such as butane, could proceed through similar C−C β-alkyl transfer for both Zr and Ta.

We previously reported on the hydrogenolysis of small alkanes, such as ethane and propane, and we proposed an α-alkyl transfer mechanism for ethane, with formation of a Ta-carbene species, since it cannot undergo β-alkyl transfer.[10] Indeed, in the case of butane, the α-alkyl transfer, corresponding to the transformation from **13** to **14** in Figure 6 has a higher energy barrier, compared to the β-alkyl transfer step **3** → **5** and **4** → **6**. This α-alkyl transfer with the formation of a metal-carbene species is not viable with bipodal Zr-species, because it would request the formation of a formal Zr(V) species.

CONCLUSIONS

In this paper, we have investigated the mechanism of *n*-butane hydrogenolysis promoted by Ta-hydride(s) supported on silica, with a particular focus on the C−C activation step. The main conclusions that can be derived from the present study are as follows:

(i) The starting monohydride $Ta^{(III)}$ can be trapped barrier less by molecular hydrogen to the corresponding tris-hydride $Ta^{(V)}$.

(ii) The addition of alkane to the metal has a remarkable low activation barrier, even in the case of highly unsaturated monohydride $Ta^{(III)}$, so that the most likely mechanism corresponds to C−H activation from the tris-hydride $Ta^{(V)}$ with concerted elimination of molecular hydrogen.

(iii) The most likely mechanism for the C−C activation step corresponds to a classic β-alkyl transfer from the Ta-alkyl moiety, with liberation of an olefin, while C−C activation through α-alkyl transfer to the metal from the Ta-alkyl ligand, with formation of a Ta-carbene species, is not competitive in large alkanes.

(iv) Nevertheless, there is a series of possible transformations, including isomerization between linear and branched alkyl Ta-species, which are faster than the productive C−C activation step through β-alkyl transfer from the Ta-alkyl species. These transformations are nonproductive and are thermodynamically biased toward bis-hydride Ta-alkyl species, from which C−C activation can start.

(v) Consistent with the experiments, there is very scarce selectivity between the activation of the Cα−Cβ or Cβ−Cβ' bonds of *n*-butane, initially leading to methane and propene, and to ethane and ethene, respectively.

(vi) Hydrogenation of the olefin (initially formed) by Ta-hydride species is an easy step, and it makes the overall process thermodynamically favored.

dx.doi.org/10.1021/cs5001703 | ACS Catal. 2014, 4, 1868−1874

(vii) Finally, the formed ethane can undergo an energetically more-expensive hydrogenolysis through α-alkyl transfer to the metal, with the formation of Ta-carbene intermediates.

■ ASSOCIATED CONTENT

Supporting Information

Cartesian coordinates and energy of all the species discussed in the text. This material is available free of charge via the Internet at http://pubs.acs.org.

■ AUTHOR INFORMATION

Corresponding Authors

*Tel.: +966-2-808-0329. Fax: +966-2-802-1025. E-mail: Luigi.Cavallo@kaust.edu.sa (L. Cavallo).

*Tel.: +966-2-808-0329. Fax: +966-2-802-1025. E-mail: Jeanmarie.basset@kaust.edu.sa (J. M. Basset).

Notes

The authors declare no competing financial interest.

■ ACKNOWLEDGMENTS

This work was supported by King Abdullah University of Science and Technology (KAUST) Saudi Arabia.

■ REFERENCES

(1) (a) Rostrup-Nielsen, J. R.; Alstrup, I. *Catal. Today* **1999**, *53*, 311−316. (b) Rana, M. S.; Samano, V.; Ancheyta, J.; Diaz, J. A. I. *Fuel* **2007**, *86*, 1216−1231.

(2) Dufaud, V. R.; Basset, J. M. *Angew. Chem., Int. Ed.* **1998**, *37*, 806−810.

(3) (a) Kochloef, K.; Bazant, V. *J. Catal.* **1967**, *8*, 250−260. (b) Bond, G. C.; Rajaram, R. R.; Burch, R. *J. Phys. Chem.* **1986**, *90*, 4877−4881. (c) Engstrom, J. R.; Goodman, D. W.; Weinberg, W. H. *J. Am. Chem. Soc.* **1988**, *110*, 8305−8319. (d) Bond, G. C.; Gelsthorpe, M. R. *J. Chem. Soc. Faraday Trans.* **1991**, *87*, 2479−2485. (e) Bond, G. C.; Calhoun, J.; Hooper, A. D. *J. Chem. Soc. Faraday Trans.* **1996**, *92*, 5117−5128. (f) Jackson, S. D.; Kelly, G. J.; Webb, G. *J. Catal.* **1998**, *176*, 225−234. (g) Bond, G. C.; Hooper, A. D. *Appl. Catal., A* **2000**, *191*, 69−81. (h) Lomot, D.; Juszczyk, W.; Karpinski, Z.; Larsson, R. *J. Mol. Catal. A—Chem.* **2002**, *186*, 163−172.

(4) (a) Lecuyer, C.; Quignard, F.; Choplin, A.; Olivier, D.; Basset, J. M. *Angew. Chem., Int. Ed.* **1991**, *30*, 1660−1661. (b) Rosier, C.; Niccolai, G. P.; Basset, J. M. *J. Am. Chem. Soc.* **1997**, *119*, 12408−12409. (c) Corker, J.; Lefebvre, F.; Lecuyer, C.; Dufaud, V.; Quignard, F.; Choplin, A.; Evans, J.; Basset, J. M. *Science* **1996**, *271*, 966−969. (d) Dornelas, L.; Reyes, S.; Quignard, F.; Choplin, A.; Basset, J. M. *Chem. Lett.* **1993**, 1931−1934. (e) Larabi, C.; Merle, N.; Norsic, S.; Taoufik, M.; Baudouin, A.; Lucas, C.; Thivolle-Cazat, J.; de Mallmann, A.; Basset, J. M. *Organometallics* **2009**, *28*, 5647−5655.

(5) Solans-Monfort, X.; Chow, C.; Goure, E.; Kaya, Y.; Basset, J. M.; Taoufik, M.; Quadrelli, E. A.; Eisenstein, O. *Inorg. Chem.* **2012**, *51*, 7237−7249.

(6) Vidal, V.; Theolier, A.; Thivolle-Cazat, J.; Basset, J. M. *Science* **1997**, *276*, 99−102.

(7) Rataboul, F.; Chabanas, M.; de Mallmann, A.; Copéret, C.; Thivolle-Cazat, J.; Basset, J. M. *Chem.—Eur. J.* **2003**, *9*, 1426−1434.

(8) Avenier, P.; Lesage, A.; Taoufik, M.; Baudouin, A.; De Mallmann, A.; Fiddy, S.; Vautier, M.; Veyre, L.; Basset, J. M.; Emsley, L.; Quadrelli, E. A. *J. Am. Chem. Soc.* **2007**, *129*, 176−186.

(9) Gavenonis, J.; Tilley, T. D. *J. Am. Chem. Soc.* **2002**, *124*, 8536−8537.

(10) Polshettiwar, V.; Pasha, F. A.; De Mallmann, A.; Norsic, S.; Thivolle-Cazat, J.; Basset, J. M. *ChemCatChem.* **2012**, *4*, 363−369.

(11) (a) Goure, E.; Avenier, P.; Solans-Monfort, X.; Veyre, L.; Baudouin, A.; Kaya, Y.; Taoufik, M.; Basset, J. M.; Eisenstein, O.; Quadrelli, E. A. *New J. Chem.* **2011**, *35*, 1011−1019. (b) Basset, J. M.; Copéret, C.; Soulivong, D.; Taoufik, M.; Cazat, J. T. *Acc. Chem. Res.* **2010**, *43*, 323−334. (c) Soulivong, D.; Norsic, S.; Taoufik, M.; Copéret, C.; Thivolle-Cazat, J.; Chakka, S.; Basset, J. M. *J. Am. Chem. Soc.* **2008**, *130*, 5044−5045. (d) Soignier, S.; Taoufik, M.; Le Roux, E.; Saggio, G.; Dablemont, C.; Baudouin, A.; Lefebvre, F.; de Mallmann, A.; Thivolle-Cazat, J.; Basset, J. M.; Sunley, G.; Maunders, B. M. *Organometallics* **2006**, *25*, 1569−1577.

(12) (a) Arney, D. S. J.; Fox, P. A.; Bruck, M. A.; Wigley, D. E. *Organometallics* **1997**, *16*, 3421−3430. (b) Fivet, V.; Biemont, E.; Engstrom, L.; Lundberg, H.; Nilsson, H.; Palmeri, P.; Quinet, P. *J. Phys. B—At. Mol. Opt.* **2008**, *41*, 015702. (c) Saggio, G.; de Mallmann, A.; Maunders, B.; Taoufik, M.; Thivolle-Cazat, J.; Basset, J. M. *Organometallics* **2002**, *21*, 5167−5171.

(13) (a) Chabanas, M.; Vidal, V.; Copéret, C.; Thivolle-Cazat, J.; Basset, J. M. *Angew. Chem., Int. Ed.* **2000**, *39*, 1962−1965. (b) Copéret, C.; Chabanas, M.; Saint-Arroman, R. P.; Basset, J. M. *Angew. Chem., Int. Ed.* **2003**, *42*, 156−181.

(14) Parr, R. G. *Density-Functional Theory of Atoms and Molecules*; Oxford University Press: Oxford, U.K., 1994; p 333.

(15) Frisch, M. J.; Trucks, G. W.; Schlegel, H. B.; Scuseria, G. E.; Robb, M. A.; Cheeseman, J. R.; Scalmani, G.; Barone, V.; Mennucci, B.; Petersson, G. A.; Nakatsuji, H.; Caricato, M.; Li, X.; Hratchian, H. P.; Izmaylov, A. F.; Bloino, J.; Zheng, G.; Sonnenberg, J. L.; Hada, M.; Ehara, M.; Toyota, K.; Fukuda, R.; Hasegawa, J.; Ishida, M.; Nakajima, T.; Honda, Y.; Kitao, O.; Nakai, H.; Vreven, T.; Montgomery, J. A.; , Jr., Peralta, J. E.; Ogliaro, F.; Bearpark, M.; Heyd, J. J.; Brothers, E.; Kudin, K. N.; Staroverov, V. N.; Kobayashi, R.; Normand, J.; Raghavachari, K.; Rendell, A.; Burant, J. C.; Iyengar, S. S.; Tomasi, J.; Cossi, M.; Rega, N.; Millam, J. M.; Klene, M.; Knox, J. E.; Cross, J. B.; Bakken, V.; Adamo, C.; Jaramillo, J.; Gomperts, R.; Stratmann, R. E.; Yazyev, O.; Austin, A. J.; Cammi, R.; Pomelli, C.; Ochterski, J. W.; Martin, R. L.; Morokuma, K.; Zakrzewski, V. G.; Voth, G. A.; Salvador, P.; Dannenberg, J. J.; Dapprich, S.; Daniels, A. D.; Farkas, Ö.; Foresman, J. B.; Ortiz, J. V.; Cioslowski, J.; Fox, D. J. *Gaussian 09*; Gaussian, Inc.: Wallingford, CT, 2009.

(16) (a) Schafer, A.; Horn, H.; Ahlrichs, R. *J. Chem. Phys.* **1992**, *97*, 2571−2577. (b) Schafer, A.; Huber, C.; Ahlrichs, R. *J. Chem. Phys.* **1994**, *100*, 5829−5835.

(17) Haussermann, U.; Dolg, M.; Stoll, H.; Preuss, H.; Schwerdtfeger, P.; Pitzer, R. M. *Mol. Phys.* **1993**, *78*, 1211−1224.

(18) Rozanska, X.; Delbecq, F.; Sautet, P. *Phys. Chem. Chem. Phys.* **2010**, *12*, 14930−14940.

(19) (a) Kresse, G.; Hafner, J. *Phys. Rev. B* **1994**, *49*, 14251−14269. (b) Kresse, G.; Furthmuller, J. *Comput. Mater. Sci.* **1996**, *6*, 15−50. (c) Kresse, G.; Furthmuller, J. *Phys. Rev. B* **1996**, *54*, 11169−11186. (d) Kresse, G.; Joubert, D. *Phys. Rev. B* **1999**, *59*, 1758−1775. (e) Kresse, G.; Hafner, J. *Phys. Rev. B* **1993**, *48*, 13115−13118.

(20) (a) Perdew, J. P.; Burke, K.; Wang, Y. *Phys. Rev. B* **1998**, *57*, 14999−. (b) Perdew, J. P.; Burke, K.; Wang, Y. *Phys. Rev. B* **1996**, *54*, 16533−16539.

(21) Blochl, P. E. *Phys. Rev. B* **1994**, *50*, 17953−17979.

(22) Avenier, P.; Taoufik, M.; Lesage, A.; Solans-Monfort, X.; Baudouin, A.; de Mallmann, A.; Veyre, L.; Basset, J. M.; Eisenstein, O.; Emsley, L.; Quadrelli, E. A. *Science* **2007**, *317*, 1056−1060.

(23) Woo, T. K.; Blochl, P. E.; Ziegler, T. *J. Phys. Chem. A* **2000**, *104*, 121−129.

(24) Chen, Y.; Credendino, R.; Callens, E.; Atiqullah, M.; Al-Harthi, M. A.; Cavallo, L.; Basset, J. M. *ACS Catal.* **2013**, *3*, 1360−1364.

(25) Mortensen, J. J.; Parrinello, M. *J. Phys. Chem. B* **2000**, *104*, 2901−2907.

(26) (a) Keitz, B. K.; Grubbs, R. H. *J. Am. Chem. Soc.* **2011**, *133*, 16277−16284. (b) Stewart, I. C.; Keitz, B. K.; Kuhn, K. M.; Thomas, R. M.; Grubbs, R. H. *J. Am. Chem. Soc.* **2010**, *132*, 8534−8535.

(27) (a) Moscardi, G.; Resconi, L.; Cavallo, L. *Organometallics* **2001**, *20*, 1918−1931. (b) Toto, M.; Cavallo, L.; Corradini, P.; Moscardi, G.; Resconi, L.; Guerra, G. *Macromolecules* **1998**, *31*, 3431−3438. (c) Talarico, G.; Busico, V.; Cavallo, L. *Organometallics* **2004**, *23*, 5989−5993. (d) Talarico, G.; Busico, V.; Cavallo, L. *J. Am. Chem. Soc.* **2003**, *125*, 7172−7173.